Fabrication of Y$_2$O$_3$-stabilized-ZrO$_2$(YSZ)/La$_{0.8}$Sr$_{0.2}$MnO$_{3-\alpha}$−YSZ dual-layer hollow fibers for the cathode-supported micro-tubular solid oxide fuel cells by a co-spinning/co-sintering technique

Xiuxia Meng [a,b], Xun Gong [a], Naitao Yang [a], Xiaoyao Tan [a,c,*], Yimei Yin [b], Zi-Feng Ma [b,*]

[a] School of Chemical Engineering, Shandong University of Technology, Zibo 255049, China
[b] School of Chemistry and Chemical Engineering, Shanghai Jiao Tong University, Shanghai 200240, China
[c] Department of Chemical Engineering, Tianjin Polytechnic University, Tianjin 300160, China

HIGHLIGHTS

► Asymmetric YSZ/LSM−YSZ dual-layer hollow fibers were prepared in a single step.
► A suitable sintering temperature range of 1350−1400 °C for the fibers was given.
► Cathode-supported MT-SOFCs were obtained by dip-coating anode on outer surface.
► A maximum power density of 290 mW cm^{-2} was obtained at 850 °C for the MT-SOFCs.
► Microstructure of the cathode layer has to be improved for higher output density.

ARTICLE INFO

ABSTRACT

Y$_2$O$_3$-stabilized-ZrO$_2$(YSZ)/La$_{0.8}$Sr$_{0.2}$MnO$_{3-\alpha}$(LSM)−YSZ dual-layer hollow fibers have been fabricated for micro-tubular solid oxide fuel cells (MT-SOFCs) using a co-spinning/co-sintering technique. The hollow fibers consist of a dense YSZ top layer supported on the porous LSM−YSZ substrate with an asymmetric structure. The electrolyte and the cathode layers are perfectly adhered to each other without observable elemental inter-diffusion. Both the mechanical strength of the hollow fibers and the compactness of the electrolyte layer are improved by increasing the sintering temperature, whereas the effective porosity of the cathode layer also decreases. The suitable sintering temperature of the YSZ/LSM−YSZ dual-layer hollow fibers to construct the electrolyte/cathode half-cells should be controlled between 1350 °C and 1400 °C. An Ni-YSZ layer of about 5 μm in thickness is dip-coated on the outer surface of the hollow fibers to serve as the anode of fuel cells. The resultant micro-tubular SOFCs yield a maximum power density of 290 mW cm^{-2} at 850 °C using 1.49 × 10^{-5} mol s^{-1} hydrogen as fuel and 2.23 × 10^{-5} mol s^{-1} air as oxidant, respectively. The output performance of the micro-tubular fuel cells is mainly limited by the high polarization resistance of the cathode.

1. Introduction

Micro-tubular solid oxide fuel cells (MT-SOFCs) have attracted increasing interest in recent years because of their unique characteristics such as large electrode area per unit volume, high volumetric power density, high mass-transfer and heat-transfer efficiency and rapid start-up/shut-down operation [1−3]. Most studies are mainly focused on the anode-supported MT-SOFCs in which the electrolyte membrane and the cathode are formed in successive on the anode microtubes [4−7], because they demonstrate high output performance. But the anode-supported SOFCs also exhibit such drawbacks as poor redox stability, carbon deposition and difficulty of stack assembly. Comparatively, the cathode-supported SOFCs are more stable and reliable in operation because the thinner anode can avoid the volume contraction and expansion resulted from anode redox cycles. Siemens Westinghouse Power (SWP) reported the successful long-term operation over 30,000 h using cathode-supported tubular SOFCs [8−11]. Furthermore, metal-based materials such as Ni can be used for current collecting in the assembly of fuel cell stacks. However, fabrication of thin electrolyte membranes on the cathode supports usually needs expensive and mass production-limited

* Corresponding authors. School of Chemical Engineering, Shandong University of Technology, Zibo 255049, China. Tel./fax: +86 533 2786292.
   E-mail addresses: cestanxy@yahoo.com.cn (X. Tan), zfma@sjtu.edu.cn (Z.-F. Ma).

Table 1
The suspension compositions for spinning the YSZ/LSM–YSZ hollow fibers.

Suspension	Composition, wt%					Viscosity at 50 s^{-1} cP
	YSZ	LSM	PESf	NMP	Ball graphite	
Cathode	22.5	33.75	8.33	29.17	6.25	19800
Electrolyte	52.17	0	8.7	39.13	—	4400

techniques (such as PVD, EVD–CVD), leading to remarkable increase in manufacturing costs of the cathode-supported tubular SOFCs. Although dip-coating followed by co-sintering is an effective way to lower the costs, it is also very difficult to fabricate a dense electrolyte film on a porous cathode due to the poor chemical compatibility of cathodes and electrolyte at high temperatures [12,13]. It is necessary to develop innovative and low-cost fabrication technologies for the commercialization of cathode-supported SOFCs.

The immersion induced phase inversion technique has been applied to fabricate various ceramic hollow fiber membranes [14–16]. The resultant hollow fibers may have an asymmetric structure consisting of a dense top layer integrated with a porous substrate. This technique has exhibited noticeable advantages to prepare MT-SOFCs over the conventional extrusion method because the dense electrolyte membrane (top layer) is formed directly on a porous substrate which can be made easily into anode by deposition of catalysts, hence the process is simplified significantly [17–21]. Recently, the phase inversion method has been modified as the co-spinning/co-sintering technique to prepare MT-SOFCs, where the anode and the electrolyte membrane are generated in a single step [22–24]. The prepared MT-SOFC exhibited highest power density of 2.32 W cm^{-2} after the anode structure was optimized [25].

In this work, Y_2O_3-stabilized-ZrO_2(YSZ)/$La_{0.8}Sr_{0.2}MnO_{3-\alpha}$(LSM)-YSZ dual-layer hollow fibers were fabricated as the electrolyte/

cathode half cells by the co-spinning/co-sintering technique. LSM was selected because it is one of the most reliable cathode materials with good stability and compatibility with YSZ electrolyte even at high operation temperatures [8]. An Ni-YSZ layer of around 5 μm in thickness was coated on the outer surface of the hollow fibers by the dip-coating and sintering method to form cathode-supported MT-SOFCs. The performances of the fuel cells associated with the microstructure of the hollow fibers were investigated experimentally.

2. Experimental

2.1. Materials

Commercially available 8 mol% yttria-stabilized zirconia (8YSZ) powders of purity 99.9% and of particle size of 20–30 nm in diameter [Weifang Yitong Co. Ltd., Weifang, China] were used as the cathode and electrolyte materials. The cathode material, $La_{0.8}Sr_{0.2}MnO_{3-\alpha}$ (LSM) was synthesized via the Pechini method. Green NiO as the anode material was purchased from Sinopharm Chemical Reagent Co., Ltd. Polyethersulfone (PESf) ((Radel A-300), Ameco Performance, USA), N-methyl-2-pyrrolidone (NMP) (AR Grade, >99.8%, Kermel Chem Inc., Tianjin, China), and commercially available ball graphite (20–30 μm in diameter) were used as the polymer binder, solvent and pore-forming agent respectively to prepare the spinning solutions. Deionized water and tap water were used as the internal and the external coagulants for spinning, respectively.

2.2. Fabrication of YSZ/LSM–YSZ hollow fibers

The phase inversion-based co-extrusion method was applied to spin the YSZ/LSM–YSZ dual-layer hollow fiber precursors. It started
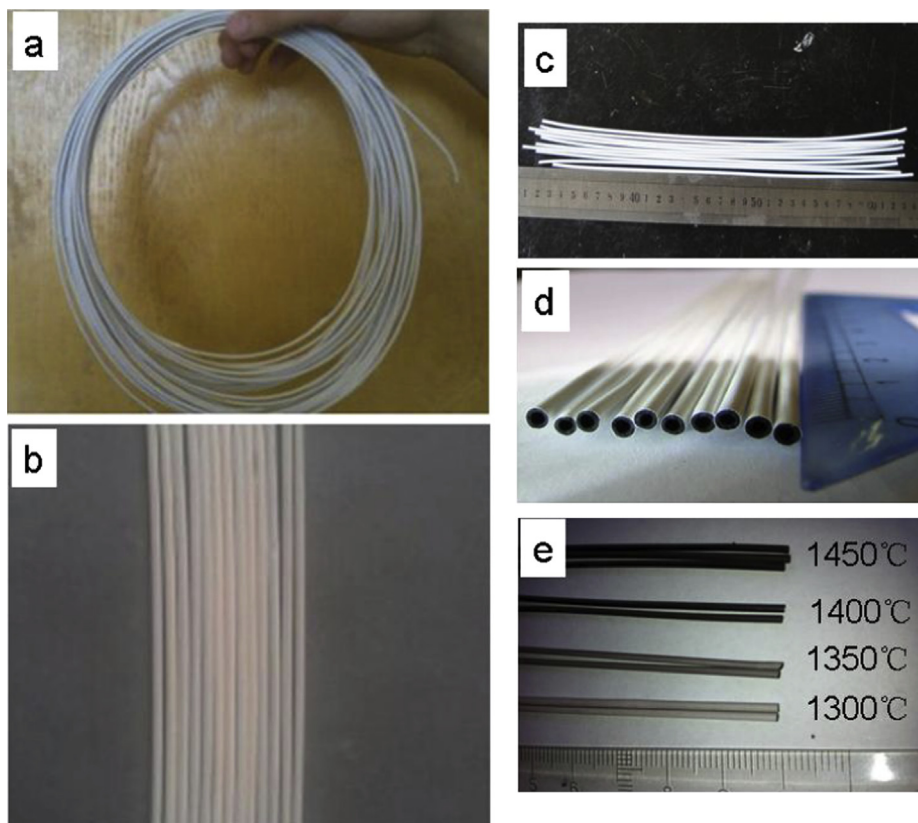
Fig. 1. Photographic images of YSZ/LSM–YSZ dual-layer hollow fiber membrane. (a) Wet precursors; (b) straight wet precursors; (c) dry precursors; (d) cross-section; and (e) sintered dual-layer HFs.

with the preparation of YSZ and LSM–YSZ suspensions. A calculated amount of PESf pellets was dissolved in NMP in a 125 cm³ wide-neck bottle to form a polymer solution. YSZ or LSM–YSZ (6:4 in weight ratio) powders, which were dried at 120 °C for 12 h in advance, were added gradually under stirring. The stirring was carried out continuously for 48 h to ensure that all the powders were dispersed uniformly in the polymer solution. Physica UDS-200 rheometer was used to measure the viscosity of the suspensions at 20 °C prior to spinning. The compositions of the YSZ and LSM–YSZ suspensions for spinning are listed in Table 1.

After degassing at room temperature for 2 h, the LSM–YSZ and the YSZ suspensions were transferred separately to two stainless steel syringes. With the help of two high-pressure pumps (LSP01-1BH, Baoding, China), the dopes were co-extruded simultaneously through a triple-orifice spinneret, passing through a 20 cm air gap, into a water coagulant bath. The extruding rates of the LSM–YSZ inner dope and the YSZ outer dope were 10 cm³ min⁻¹ and 2 cm³ min⁻¹, respectively, while the internal coagulant flow rate was controlled at 14 cm³ min⁻¹. The hollow fibers were retained in the external coagulation bath so as to complete the solidification process. After 24 h, the hollow fiber precursors were taken out of the water bath, cut into pieces of about 30 cm long, straightened and dried at room temperature successively. Finally, a high-temperature sintering was conducted on the hollow fiber precursors in ambient non-flowing air atmosphere for 10 h to obtain gastight YSZ/LSM–YSZ dual-layer hollow fibers. The hollow fibers at different stages are shown in Fig. 1. The gastight property of the sintered hollow fibers was measured using a N_2 permeation test described elsewhere [26].

2.3. Fabrication and performance measurement of MT-SOFCs

The gastight hollow fibers were cut into microtubes with the length of about 5 cm. A coating suspension was prepared with anode powders (60 wt.% NiO-8YSZ), solution, binder, surfactant, plasticizer, lubricant etc. the anode powders and surfactant triethanolamine (TEA) were added into the ethanol (EtOH)/methyl ethyl ketone (MEK) azeotrope (EtOH/MEK = 1/2). After ball-milling

for 24 h, the binder polyvinylbutyral (PVB), plasticizer Di-butyl-phthalate (DBP) and lubricant polyethylene glycol (PEG) were added and ball-milled for another 24 h. Dip-coating was performed on a pulling machine (TL0.01, Shenyang Kejing Instruments Co. Ltd). Prior to coating, one end of the dual-layer hollow fiber was sealed with epoxy resin. The fiber was dipped into the suspension and then pulled out with a rate of 20 mm min⁻¹. After drying at room temperature for 1 h, the dip-coating–pulling–drying process was repeated. At last the fiber coated with green NiO-YSZ membrane was moved to a furnace and dried at 100 °C for 12 h, followed by sintering at 1200 °C for 2 h.

For the measurement of fuel cell performance, a silver wire was wrapped around the outer anode while another one was looped inside the fiber lumen as the current collectors. Ag paste diluted by ethanol was coated by brushing and flushing on the anode and cathode surfaces respectively to reduce the electrical resistance. Concurrently, conductive Ag paste was used to fix the silver wires onto the electrode surfaces. The fuel cell with current collectors connected to two small quartz tubes on both ends with a silver-based high-temperature sealant was housed in a large quartz tube, as shown in Fig. 2. A K-type thermocouple was used to monitor the operation temperature. The error of the temperature controlling system was ±1 °C. Before the measurement, the anode was reduced by flowing hydrogen on the shell side at 700 °C for 1 h. I–V & I–P curves of the cells were collected using a DC Electronic Load (Keithley 2440-5A) at 700–850 °C with hydrogen as the fuel and air as the oxidant. The flow rates of hydrogen and air were fixed at 1.49×10^{-5} mol s⁻¹ and 2.23×10^{-5} mol s⁻¹, respectively. Resistances of the cell under open circuit condition were measured by an electrochemistry workstation (Zahner IM6ex, Germany) with the frequency was sweeping from 1 M to 0.01 Hz with amplitude of 10 mV.

2.4. Characterization

Microstructures of the hollow fibers were ascertained by scanning electron microscopy (SEM) (FEI Sirion200, The Netherlands). Gold sputter coating was performed on the samples under vacuum before the measurements. The crystal phases of the prepared dual-
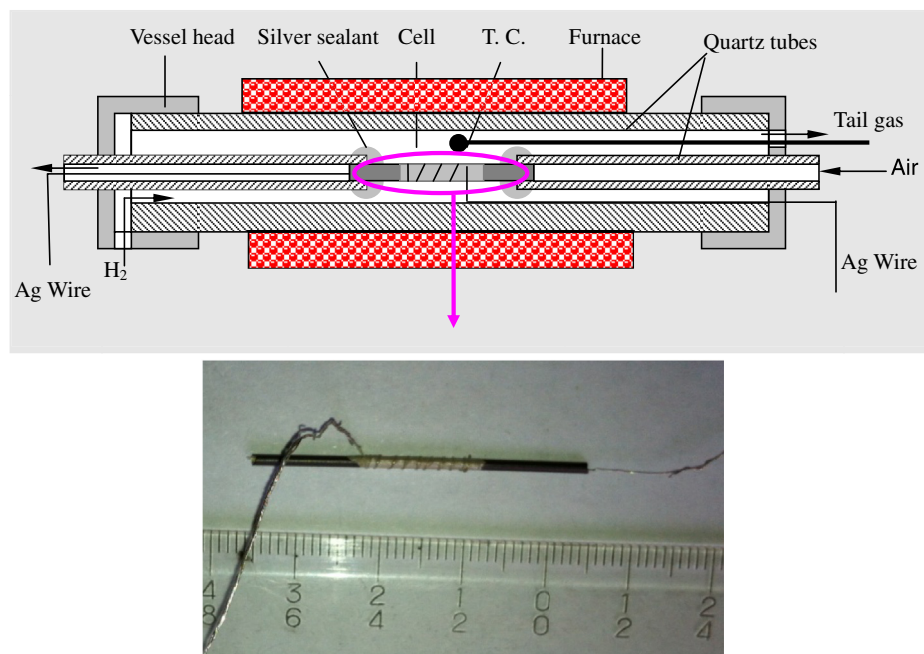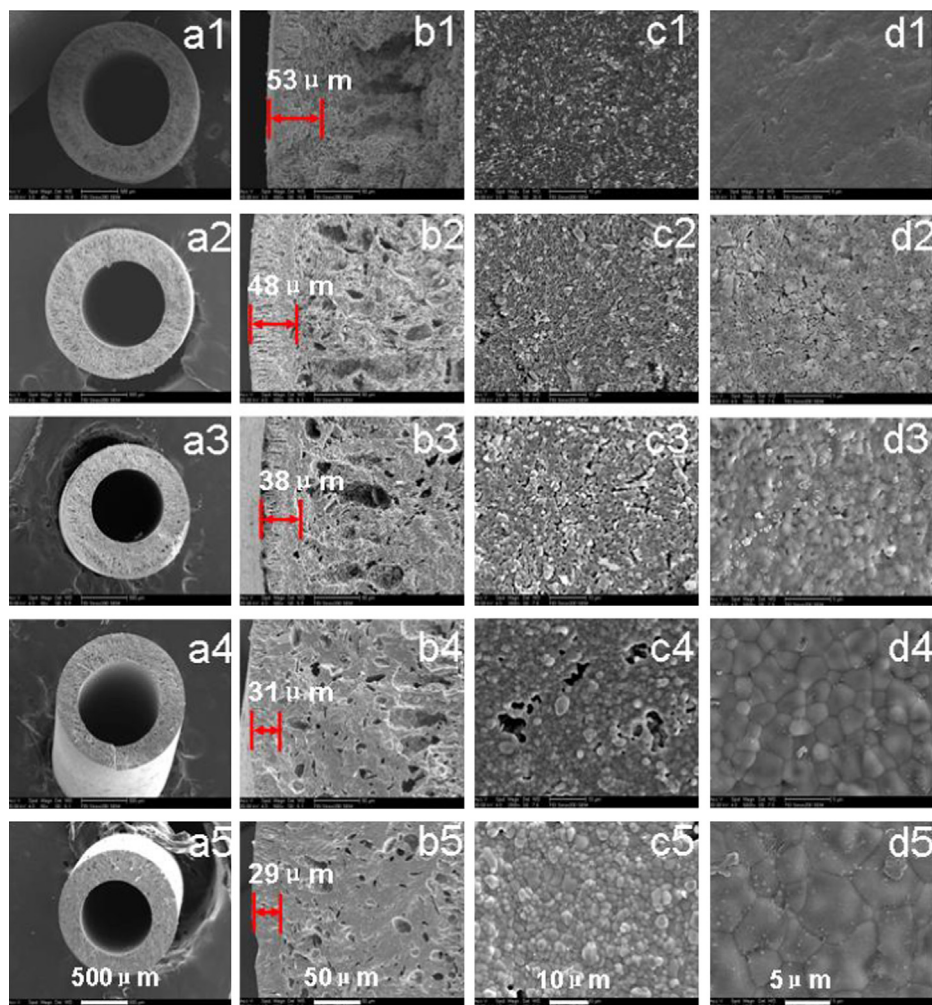

Fig. 2. (a) Schematic diagram and (b) photographic image of the assembled single MT-SOFC.

Fig. 3. SEM images of the YSZ/LSM—YSZ dual-layer hollow fibers. 1-Precusors; 2-sintered at 1300 °C; 3-sintered at 1350 °C; 4-sintered at 1400 °C; 5-sintered at 1450 °C; (a) cross-section; (b) magnified cross-section; (c) inner surface; and (d) outer surface.

layer hollow fibers were determined by X-ray diffraction (BRUKER D8 Advance, Germany) using Cu Kα radiation ($\lambda = 0.15404$ nm). Continuous scan mode was used to collect 2θ data from 20° to 80° with a 0.02° sampling pitch and a 2°min^{-1} scan rate. The X-ray tube voltage and current were set at 40 kV and 30 mA, respectively. The porosity was measured by Archimedes method.

The mechanical strength of the hollow fibers was measured on a three-point bending instrument (Instron Model 5544) with a crosshead speed of 0.5 mm min^{-1}. Hollow fiber samples were fixed

on the sample holder at a distance of 32 mm. The bending strength, σ_F, was calculated from the following equation:

$$\sigma_F = \frac{8FLD}{\pi(D^4 - d^4)} \tag{1}$$

where F is the measured force at which fracture takes place; L, D and d are the length (32 mm), the outer diameter and the inner diameter of the hollow fibers, respectively. The values of outer
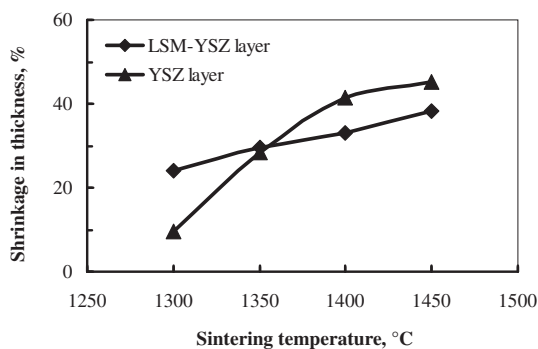
Fig. 4. Shrinkage of the cathode and electrolyte layers in YSZ/LSM—YSZ dual-layer hollow fibers as a function of sintering temperature.
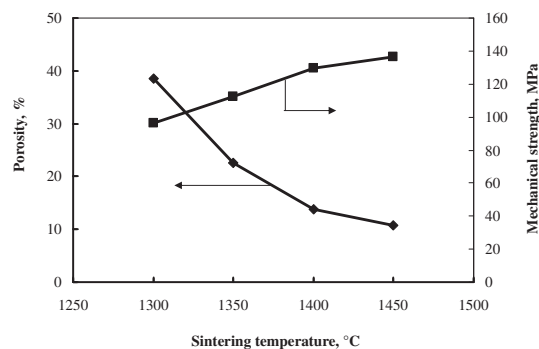
Fig. 5. Porosity and mechanical strength of the YSZ/LSM—YSZ dual-layer hollow fibers as a function of sintering temperature.
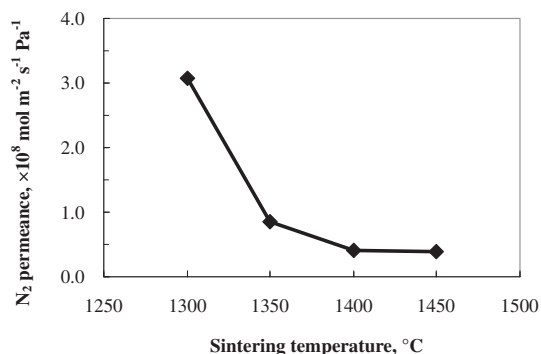
Fig. 6. N_2 permeance through the YSZ/LSM–YSZ dual-layer hollow fibers sintered at different temperatures.

diameter (D) and inner diameter (d) were obtained from the SEM graphs.

3. Results and discussions

3.1. YSZ/LSM–YSZ dual-layer hollow fibers

Fig. 3 shows the SEM images of the YSZ/LSM–YSZ dual-layer hollow fibers sintered at different temperatures. The cross-section of the hollow fiber precursor (Fig. 3 (a1)) exhibits an asymmetric structure consisting of a porous LSM–YSZ inner layer

and a relatively dense YSZ outer layer. There are many macro voids formed within the LSM–YSZ layer (Fig. 3 (b1)) because of the phase separation of the PESf-contained dope occurring as the non-solvent diffuses into the nascent fiber wall. Furthermore, instantaneous phase separation or liquid–liquid demixing takes place on the outer surface as soon as the spinning solution extruded from the spinneret contacts with water, leading to the formation of a dense skin layer on the outer surface side as shown in (Fig. 3 (d1)). However, the inner surface (Fig. 3 (c1)) is not so smooth as the outer surface because the precipitation rate occurring on the inner surface is slower than that on the outside surface due to the lower non-solvent concentration in the internal coagulant. No distinct interface is observed between the outer YSZ layer and the inner LSM–YSZ layer, but the thickness of the YSZ layer still can be estimated to be ca. 53 μm. In addition, all these figures indicate that the inorganic particles are well dispersed in the hollow fiber walls.

Microstructures of the YSZ/LSM–YSZ dual-layer hollow fibers sintered at different temperatures for 10 h are shown in Fig. 3 (a2–d5), respectively. As can be seen, the general asymmetric structure of the hollow fiber precursors has not been changed during the sintering process whereas the boundary of the YSZ electrolyte layer becomes more distinct. This implies that the general structure of the hollow fibers is mainly determined in the spinning and phase inversion process. As the sintering temperature is increased, the YSZ layer has become denser and thinner while the YSZ grain has grown bigger, as is shown in Fig. 3 (d2–d5). The thickness of the YSZ layer decreases from the initial ca. 53 μm of the hollow fiber precursor to about 48 μm, 38 μm, 31 μm and 29 μm after sintering at 1300 °C, 1350 °C, 1400 °C and 1450 °C, respectively. Likewise, the
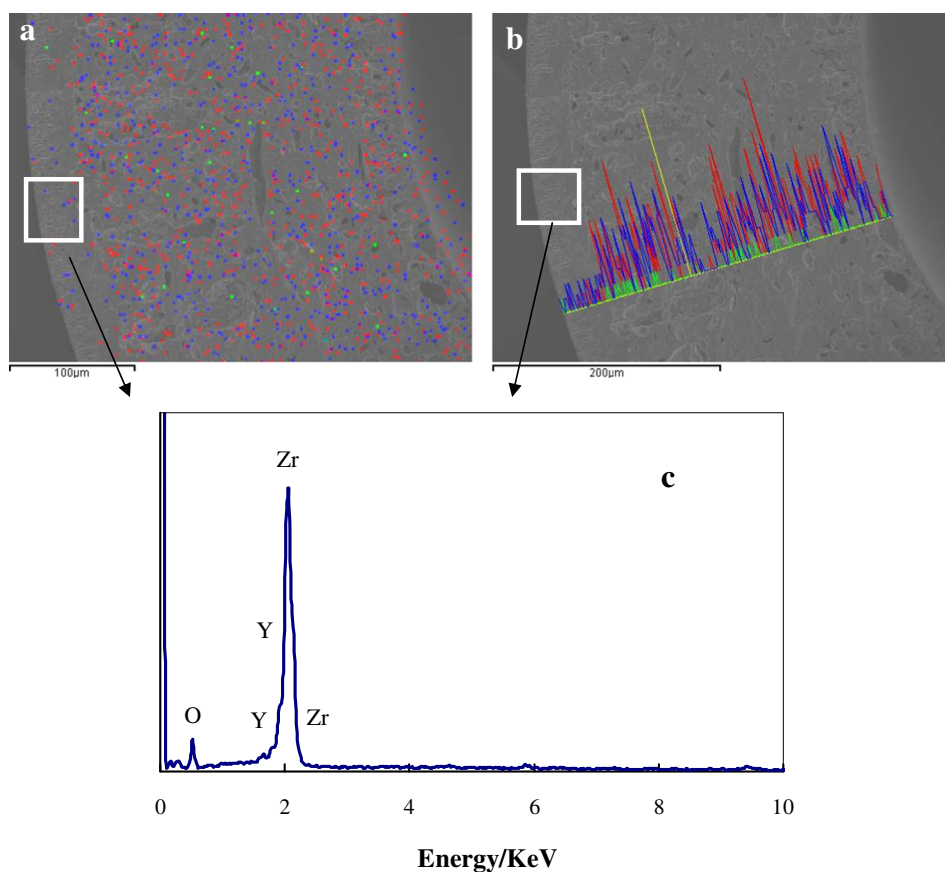
Fig. 7. Energy dispersive spectrometry (EDS) analysis of the La (blue), Sr (green) and Mn (red) distribution on the across-section and in the electrolyte layer of the YSZ/LSM–YSZ dual-layer hollow fibers sintered at 1350 °C; (A) mapping; (b) line distribution; (c) point distribution of electrolyte. [For interpretation of color referred in this figure legend, the reader is referred to web version of the article.]
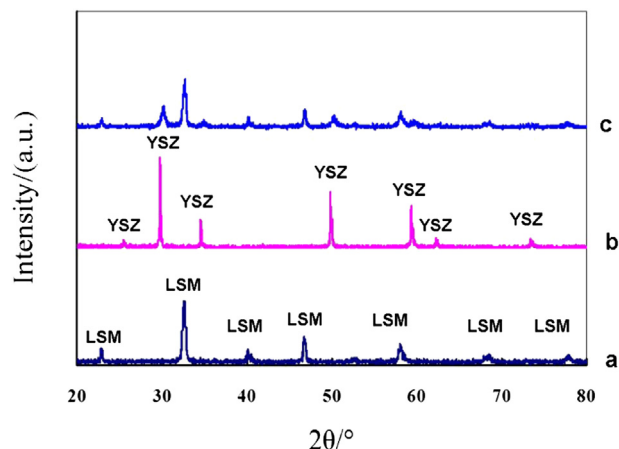
Fig. 8. XRD patterns of (a) LSM powder; (b) the outer electrolyte surface and (c) the inner cathode surface of the YSZ/LSM−YSZ dual-layer hollow fibers.

inner LSM−YSZ cathode layer also shrinks with increasing the sintering temperature. Fig. 4 shows the shrinkage of the electrolyte and the cathode layers in average thickness as a function of sintering temperature. It can be seen that the shrinkage of the LSM−YSZ layer is as much as 25.04% at 1300 °C and then increases with increasing the sintering temperature. For the cathode-supported cells, the supporting cathode dominates the densification of the supported electrolyte film due to the much thicker cathode layer than the electrolyte and anode layers [3]. The large shrinkage of the cathode support is helpful for the densification of the electrolyte film during the co-sintering process. Moreover, the YSZ electrolyte layer exhibits larger shrinkages than the cathode layer especially after the sintering temperature is higher than 1350 °C. Therefore, the YSZ electrolyte layer is integrated perfectly with the LSM-YSZ inner layer, as is observed from the SEM images of Fig. 3. This also suggests that the sintering temperature of the YSZ/LSM−YSZ dual-layer hollow fibers should be sintered at temperatures higher than 1350 °C.

Fig. 5 shows the porosity and mechanical strength of the hollow fibers as a function of sintering temperature. As can be seen, the porosity of the hollow fibers significantly decreases from 38.5% to 10.8% while the three-point bending strength increases from 96.38 MPa to 136.24 MPa as the sintering temperature is increased from 1300 °C to 1450 °C. This trend is in accordance with the changes of the shrinkage of the hollow fibers. Generally a high porosity is expected for the fast transport of oxidant in cathode layer, and hence for obtaining high fuel cell performances.

Therefore, a too high sintering temperature should not be applied in view of the cathode porosity. However, the applied sintering temperature also should be high enough to guarantee the densification of the electrolyte layer and to obtain sufficient mechanical strength. Fig. 6 shows the gastightness property of the hollow fibers in terms of N_2 permeance as a function of sintering temperature. As can be seen, the N_2 permeance through the hollow fibers decreases remarkably from 3.07×10^{-8} mol m^{-2} s^{-1} Pa^{-1} to 0.85×10^{-8} mol m^{-2} s^{-1} Pa^{-1} as the sintering temperature is increased from 1300 °C to 1350 °C. But further increase of sintering temperature from 1400 °C to 1450 °C results in negligible decrease in the N_2 permeance, i.e. 0.41×10^{-8} mol m^{-2} s^{-1} Pa^{-1}. This implies that the sintering temperature could not be higher than 1400 °C for the densification of the YSZ electrolyte layer otherwise the porosity of the cathode will be noticeably reduced. As can be seen from the SEM images (Fig. 3 (c5)), the inner surface has also become dense after the hollow fiber was sintered at 1450 °C. This is obviously not desired for the mass-transfer in the cathode. In this work, we will only use the hollow fibers sintered at 1350 °C and 1400 °C for the fabrication of fuel cells.

For the co-sintering of the electrolyte/cathode hollow fibers, the inter-layer diffusion must be avoided since it may lead to short-circuit and loss of cell efficiency. Fig. 7 shows the elemental distributions on the across-section and in the electrolyte layer of the YSZ/LSM−YSZ dual-layer hollow fibers sintered at 1350 °C for 10 h measured by energy dispersive spectrometry (EDS). As can be seen in Fig. 7 (A and B), the cathode elements, La, Sr and Mn almost are not detected in the outer electrolyte layer, indicating that these elements do not pass through the interface and diffuse into the electrolyte layer during the co-sintering process. This has also been confirmed by focusing the EDS characterization on the YSZ electrolyte layer (Fig. 7(C)). Furthermore, the La, Sr and Mn flat distribution curves show that the LSM and YSZ particles are mixed homogeneously in the cathode layer. Fig. 8 shows the X-ray diffraction (XRD) patterns of the YSZ/LSM−YSZ dual-layer hollow fibers performed on the inner cathode surface and the outer electrolyte surface. As can be seen, no impurities have appeared on the outer electrolyte surface except the YSZ phase, and on the inner surface except the LSM and YSZ phases. This further confirms that the LSM phase has not entered into the electrolyte layer of the hollow fibers.

3.2. Performance of the cathode-supported MT-SOFCs

A NiO−YSZ anode layer of 1 cm in length was dip-coated on the outer surface of the YSZ/LSM−YSZ dual-layer hollow fibers to form micro-tubular fuel cells. Fig. 9 shows the cross-sectional SEM
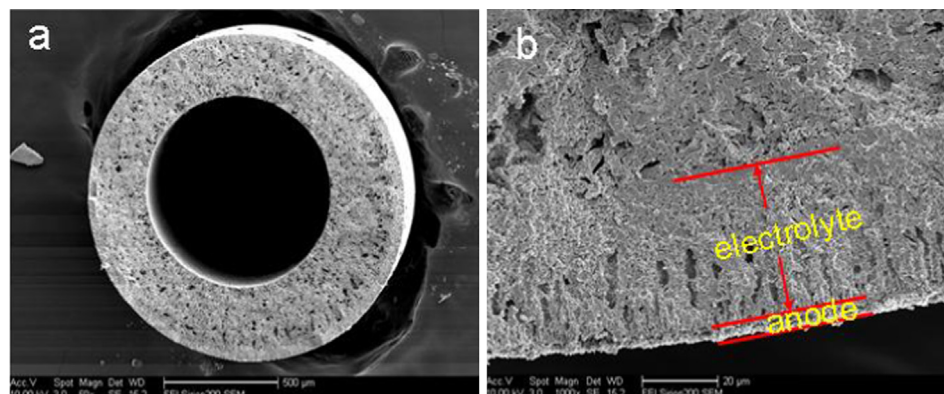

Fig. 9. Cross-sectional SEM images of the Ni-YSZ/YSZ/LSM−YSZ micro-tubular SOFC sintered at 1350 °C (a) cross-section; (b) magnified electrolyte and anode.

images of a fabricated cell made from the hollow fiber sintered at 1350 °C. As can be seen, there are some short finger pores in the electrolyte and the coated anode is only around 5 μm in thickness but is integrated well with the hollow fiber substrate.

Fig. 10 shows the output performances of the micro-tubular fuel cells using 1.49×10^{-5} mol s^{-1} hydrogen as fuel and 2.23×10^{-5} mol s^{-1} air as oxidant, respectively. It can be seen that the 1350 °C-sintered hollow fiber fuel cell had distinctly lower open circuit voltages (OCVs) than the fuel cell based on the 1400 °C-sintered hollow fibers, which demonstrated the OCVs close to the theoretical values, i.e 1.06 V at 700 °C and 0.98 V at 850 °C, respectively. This indicates that the electrolyte has become denser as the sintering temperature was increased from 1350 °C to 1400 °C. However, the higher sintering temperature may also lead to the over-sintering of the cathode of the hollow fibers. As a result, the 1400 °C-sintered hollow fiber fuel cell even gave lower power densities than the 1350 °C-sintered one especially at lower temperatures. As can be seen, the 1350 °C- and 1400 °C-sintered hollow fiber fuel cells exhibited the maximum power densities of 290 mW cm^{-2} and 283 mW cm^{-2} at 850 °C, respectively. These output values are not so high as those reported on other cathode-supported fuel cells in literature [9,12], which can be attributed to the low effective porosity in the cathode layer of the hollow fibers.

The impedance spectra of the micro-tubular fuel cells gathered under open circuit conditions are shown in Fig. 11, where the equivalent circuit for analysis is also plotted as the inset of (a). As can be seen, the ohmic resistance (R_o) of the 1350 °C-sintered hollow fiber cell is larger than that of the 1400 °C-sintered one because of the less compactness of the electrolyte layer. However, the 1400 °C-sintered hollow fiber cell exhibits larger polarization resistance (R_p) than the 1350 °C-sintered cell due to the less porosity in the cathode layer. Since the output performance of hollow fiber cell may be mainly limited by the polarization
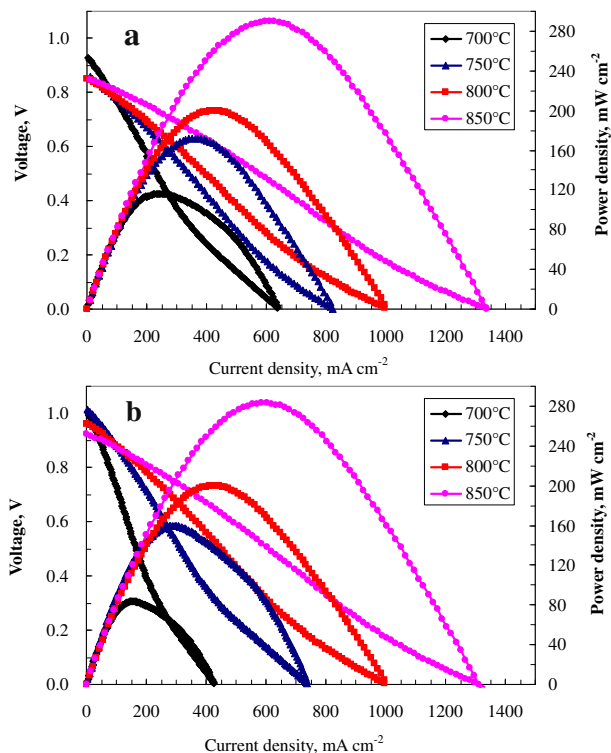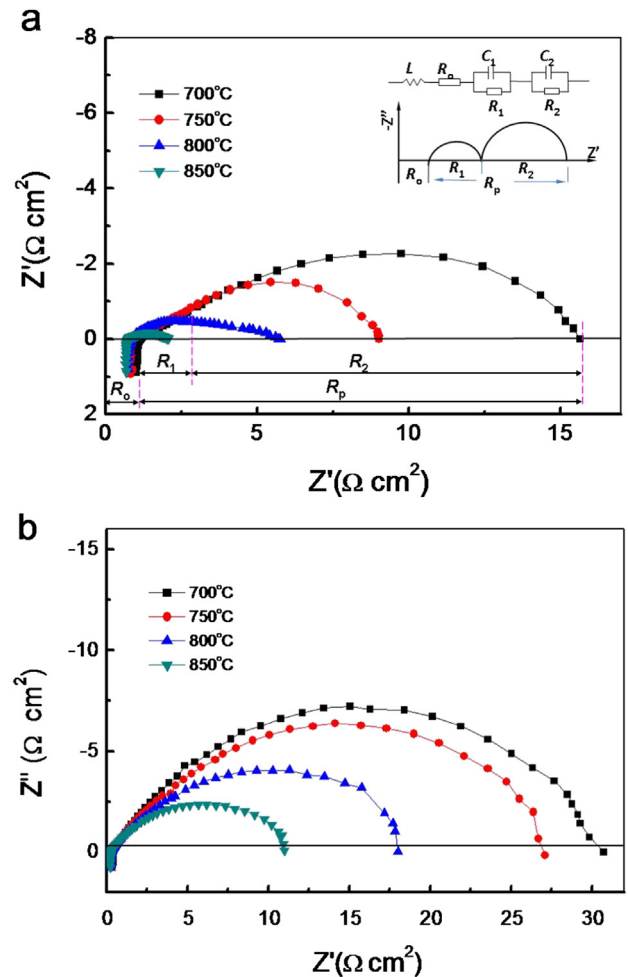

Fig. 11. EIS spectra of (a) the 1350 °C- and (b) the 1400 °C-sintered hollow fiber fuel cells at different temperatures under open circuit condition.

resistance, the 1400 °C-sintered cell exhibited lower power density than the 1350 °C-sintered one, as is shown in Fig. 10. Therefore, the improvement of the microstructure of the cathode layer of the dual-layer hollow fibers may be the greatest challenge in order to increase the output performance of the cathode-supported micro-tubular fuel cells.

4. Conclusions

Asymmetric YSZ/LSM–YSZ dual-layer hollow fibers consisting of a dense YSZ top layer supported on the LSM–YSZ substrate have been successfully prepared by the co-spinning/co-sintering technique. With increasing the sintering temperature, both the mechanical strength of the hollow fibers and the compactness of the electrolyte layer are improved while the porosity of the cathode layer decreases. In order to obtain the hollow fibers suitable for constructing the electrolyte/cathode half cells, the sintering temperature should be controlled between 1350 and 1400 °C. MT-SOFCs were fabricated by dip-coating 60 wt.% NiO–YSZ on the outer surface of the prepared dual-layer hollow fibers. The resultant MT-SOFCs exhibited maximum power density of 290 mW cm^{-2} at 850 °C using 1.49×10^{-5} mol s^{-1} hydrogen as feed and 2.23×10^{-5} mol s^{-1} air as oxidant, respectively. The performance of the fuel cells is mainly limited by the high polarization resistance of the cathode.

Fig. 10. Output performances of the Ni-YSZ/YSZ/LSM–YSZ micro-tubular fuel cells based on the hollow fibers sintered (a) at 1350 °C and (b) at 1400 °C (H$_2$ feed flow rate = 1.49×10^{-5} mol s^{-1}; air feed flow rate = 2.23×10^{-5} mol s^{-1}).

Acknowledgement

References

[1] K. Kendall, M. Palin, J. Power Sources 71 (1998) 268–270.
[2] V. Lawlor, S. Griesser, G. Buchinger, A.G. Olabi, S. Cordiner, D. Meissner, J. Power Sources 193 (2009) 387–399.
[3] K. Kendall, Int. J. Appl. Ceramic Technol. 7 (1) (2010) 1–9.
[4] Y.W. Sin, K. Galloway, B. Roy, M.N. Sammes, J.H. Song, T. Suzuki, M. Awano, Int. J. Hydrogen Energy 36 (2) (2011) 1882–1889.
[5] K.S. Howe, A.R. Hanifi, K. Kendall, M. Zazulak, T.H. Etsell, P. Sarkar, Int. J. Hydrogen Energy 38 (2013) 1058–1067.
[6] V. Gil, J. Gurauskis, R. Campana, R.I. Merino, A. Larrea, V.M. Orera, J. Power Sources 196 (2011) 1184–1190.
[7] C. Yang, W. Li, S. Zhang, L. Bi, R. Peng, C. Chen, W. Liu, J. Power Sources 187 (1) (2009) 90–92.
[8] T. Yamaguchi, S. Shimizu, T. Suzuki, Y. Fujishiro, M. Awano, Electrochemistry Commun. 10 (2008) 1381–1383.
[9] C. Zhao, R. Liu, S. Wang, Z. Wang, J. Qian, T. Wen, J. Power Sources 192 (2009) 552–555.
[10] T. Yamaguchi, S. Shimizu, T. Suzuki, Y. Fujishiro, M. Awano, Mater. Lett. 62 (2008) 1518–1520.
[11] Y. Liu, M. Mori, Y. Funahashi, Y. Fujishiro, A. Hirano, Electrochemistry Commun. 9 (2007) 1918–1923.
[12] S. Zhang, L. Bi, L. Zhang, C. Yang, H. Wang, W. Liu, Int. J. Hydrogen Energy 34 (2009) 7789–7794.
[13] B. Lin, W. Sun, K. Xie, Y. Dong, D. Dong, X. Liu, J. Gao, G. Meng, J. Alloys Compounds 465 (2008) 285–290.
[14] X. Tan, Y. Liu, K. Li, Ind. Eng. Chem. Res. 44 (2005) 61–66.
[15] Z. Wang, N. Yang, B. Meng, X. Tan, Ind. Eng. Chem. Res. 48 (2009) 510–516.
[16] W. Yin, B. Meng, X. Meng, X. Tan, J. Alloys Compounds 476 (2009) 566–570.
[17] N.T. Yang, X.Y. Tan, Z.F. Ma, J. Power Sources 183 (2008) 14–19.
[18] W. Sun, N. Zhang, Y. Mao, K. Sun, Electrochemistry Commun. 20 (2012) 117–120.
[19] C. Jin, C. Yang, F. Chen, J. Membr. Sci. 363 (2010) 250–255.
[20] L. Zhao, X.Z. Zhang, B.B. He, B.B. Liu, C.R. Xia, J. Power Sources 196 (2011) 962–967.
[21] N.T. Yang, X. Tan, X.X. Meng, Y. Yin, Z.F. Ma, Fabrication of anode supported micro tubular SOFCs by dip-coating process on NiO/YSZ hollow fibers [C] 216th ECS Meeting in Vienna, Austria, ECS Transaction 25 (2) (2009) 811–888.
[22] N. Droushiotis, Z.T. Wu, G. Kelsall, K. Li, Adv. Mater. 23 (2011) 2480–2483.
[23] M.H.D. Othman, Z.T. Wu, N. Droushiotis, D. Uttam, G. Kelsall, K. Li, J. Membr. Sci. 351 (2010) 196–204.
[24] M.H.D. Othman, N. Droushiotis, Z. Wu, G. Kelsall, K. Li, J. Power Sources 196 (2011) 5035–5044.
[25] M.H.D. Othman, N. Droushiotis, Z. Wu, G. Kelsall, K. Li, J. Power Sources 205 (2012) 272–280.
[26] X. Tan, Y. Liu, K. Li, AIChE J. 51 (2005) 1991–2000.